

# Structural and biochemical studies of the 5'→3' exoribonuclease Xrn1

Jeong Ho Chang<sup>1,3</sup>, Song Xiang<sup>1-3</sup>, Kehui Xiang<sup>1</sup>, James L Manley<sup>1</sup> & Liang Tong<sup>1</sup>

The 5'→3' exoribonucleases (XRNs) have important functions in transcription, RNA metabolism and RNA interference. The structure of Rat1 (also known as Xrn2) showed that the two highly conserved regions of XRNs form a single, large domain that defines the active site of the enzyme. Xrn1 has a 510-residue segment after the conserved regions that is required for activity but is absent from Rat1/Xrn2. Here we report the crystal structures of *Kluyveromyces lactis* Xrn1 (residues 1–1,245, E178Q mutant), alone and in complex with a Mn<sup>2+</sup> ion in the active site. The 510-residue segment contains four domains (D1–D4), located far from the active site. Our mutagenesis and biochemical studies show that their functional importance results from their ability to stabilize the conformation of the N-terminal segment of Xrn1. These domains might also constitute a platform that interacts with protein partners of Xrn1.

The 5'→3' XRNs belong to a family of conserved enzymes in eukaryotes and have important functions in transcription, RNA metabolism and RNA interference. In fungi and animals, two XRNs have been identified. Xrn1 (175 kDa) is primarily cytosolic and is involved in the degradation of decapped mRNAs, nonsense-mediated decay and microRNA decay, and is essential for proper development<sup>1–5</sup>. The Xrn1 homolog in *Drosophila*, known as Pacman, is required for male fertility<sup>6</sup>.

Xrn2 (115 kDa) is primarily nuclear, and its ortholog in *Saccharomyces cerevisiae*, more commonly known as Rat1, was initially suggested to have roles in RNA trafficking from the nucleus to the cytoplasm<sup>7,8</sup> and in transcription of some genes by RNA polymerase III (Pol III)<sup>9</sup>. More recent studies have identified Xrn2 as the exoRNase that is crucial for transcription termination by Pol II<sup>10–13</sup> and Pol I<sup>14,15</sup> according to the 'torpedo' model. Rat1/Xrn2 also promotes telomere elongation<sup>16</sup> and (together with Xrn1) the degradation of hypomodified mature tRNAs<sup>17</sup>. The Rat1/Xrn2 ortholog in *Schizosaccharomyces pombe* is required for proper chromosome segregation<sup>18</sup>. Of the three homologs of Xrn2 in the plant *Arabidopsis*, two function in the nucleus as suppressors of RNA silencing<sup>19</sup>, whereas the third functions in the cytoplasm in the ethylene response pathway<sup>20,21</sup> and in RNA interference<sup>22</sup>.

XRNs share two highly conserved regions (CR1 and CR2), corresponding to residues 1–354 and 426–595 of human Xrn1 (Fig. 1), with 58% sequence identity among the Xrn2 proteins and 48% identity between Xrn1 and Xrn2 (Supplementary Fig. 1). A cluster of seven conserved acidic residues in CR1<sup>23,24</sup> is expected to coordinate two metal ions for catalysis<sup>25</sup>. In comparison, conservation of residues outside CR1 and CR2 is much weaker. However,

the poorly conserved segment of about 120 residues just after CR2 is required for the function of Rat1/Xrn2 (ref. 18).

Xrn1 is larger than Xrn2 because it has a much longer C-terminal segment, most of which is unique to Xrn1 (Fig. 1). Weak sequence conservation among Xrn1 proteins is observed up to residue 1,180 of human Xrn1 or 1,240 of *S. cerevisiae* and *K. lactis* Xrn1 (Supplementary Fig. 1). This weakly conserved segment of approximately 570 residues is required for the nuclease activity of Xrn1. A C-terminal truncation mutant of *S. cerevisiae* Xrn1, in which residues 1,206–1,528 are removed and therefore only the last 40 residues of this segment are lacking, could not complement the growth defect in *xrn1* null cells and had essentially no exonuclease activity *in vitro*<sup>23</sup>.

The crystal structure of *S. pombe* Rat1/Xrn2 in complex with its activating partner Rai1 (ref. 26) revealed that the two conserved regions of XRNs form a single, large domain. The poorly conserved segment directly after CR2 has tight interactions with CR1, and it also mediates recruitment of Rai1 (refs. 26–28). However, it is not known whether Xrn1 has a structurally equivalent segment or, more importantly, why the 570-residue segment that follows CR2 in Xrn1 is required for activity.

We report here the crystal structures at 2.9-Å resolution of *K. lactis* Xrn1 (residues 1–1,245, E178Q mutant), alone and in complex with a Mn<sup>2+</sup> ion in the active site. The 570-residue segment that follows CR2 consists of two parts—a 60-residue segment directly after CR2 that has some similarity to the 120-residue C-terminal segment of Rat1/Xrn2, and a 510-residue segment that contains four additional domains (D1–D4). The four domains are located far from the active site but may help to stabilize the N-terminal segment of Xrn1 for catalysis.

<sup>1</sup>Department of Biological Sciences, Columbia University, New York, New York, USA. <sup>2</sup>Present address: Key Laboratory of Nutrition and Metabolism, Institute for Nutritional Sciences, Shanghai Institutes for Biological Sciences, Chinese Academy of Sciences, Shanghai 200031, P.R. China. <sup>3</sup>These authors contributed equally to this work. Correspondence should be addressed to L.T. (ltong@columbia.edu).

Received 22 August 2010; accepted 22 November 2010; published online 6 February 2011; doi:10.1038/nsmb.1984

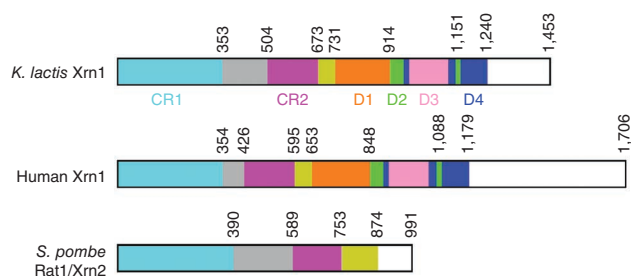


**Figure 1** Domain organization of Xrn1. Schematic drawing of the domain organizations of *K. lactis* Xrn1, human Xrn1 and *S. pombe* Rat1/Xrn2. The various domains are labeled.

## RESULTS

### Structure determination

After screening Xrn1 proteins from various organisms, we purified and crystallized residues 1–1,245 of *K. lactis* Xrn1, which cover the entire conserved region of Xrn1 (Fig. 1). The quality of these crystals was poor, with diffraction typically to about 3.2-Å resolution. We were able to locate four molecules of Xrn1 by the molecular replacement method, using the structure of *S. pombe* Rat1/Xrn2 as the search model<sup>26</sup>. We also obtained primary phasing with the selenomethionyl single-wavelength anomalous diffraction method<sup>29</sup> and improved the phase information through fourfold noncrystallographic symmetry averaging. We discovered that the E178Q mutant produced better crystals, and by screening many of them we were able to extend the resolution to 2.9 Å. This mutation is in the active site of Xrn1 and is expected to disrupt the nuclease activity<sup>23</sup>. By co-crystallizing with MnCl<sub>2</sub>, we also obtained the structure at 2.9 Å resolution of this mutant in complex with a Mn<sup>2+</sup> ion in the active site.

The refined structures agreed well with the crystallographic data and the expected bond lengths, bond angles and other geometric parameters (Table 1). The four molecules of Xrn1 had roughly the same conformation, with an r.m.s. distance of 0.8 Å for equivalent Cα atoms between any pair of the molecules. Most of the residues (82%) were in the most favored region of the Ramachandran plot, and 16% were in the additionally allowed region. The current atomic model for *K. lactis* Xrn1 contains most of the residues of the recombinant protein. Residues 1–2, 47–53, 116–127, 230–238, 409–411, 463–468, 488–503, 520–525, 609–620, 628–640, 776–780, 983–1,082 and 1,241–1,245 were omitted owing to lack of electron density (Supplementary Fig. 1).

### Overall structure of Xrn1

Residues 3–1,240 of *K. lactis* Xrn1 form a compact structure overall, in the shape of a rectangular box, with dimensions of 80 Å × 60 Å × 35 Å (Fig. 2a). Only the linker segment (residues 354–503) between the two conserved regions and residues 979–1,109 (domain D3, see below) are positioned outside this overall compact structure (Fig. 2b).

Residues in CR1 (1–353) are located in the center of the structure of Xrn1 (Fig. 2a). CR2 (residues 505–673) surrounds one side of CR1, forming one edge of the box and helping to define the active site landscape (Fig. 2a). Residues 732–1,240 at the C terminus of the recombinant protein surround the other side of CR1. This 510-residue segment is unique to Xrn1 and has no equivalents in Rat1/Xrn2 (see below). On the other hand, residues 674–731 of Xrn1, which directly follow CR2 in the primary sequence, form a long, extended structure that has some similarity to the equivalent segment of Rat1/Xrn2 (see below).

The segment that is poorly conserved between CR1 and CR2 forms a distinct domain in this structure, connected to CR1 through a 13-turn, 70-Å-long helix that places the domain far away from the

rest of the structure (Fig. 2b). The domain contains a three-stranded antiparallel β-sheet with helices on one face. Many of the loops in this domain, as well as the loop that connects it to CR2, are disordered. This domain mediates the formation of a dimer in the crystal (Supplementary Fig. 2). This dimer is probably a crystal-packing artifact, as gel-filtration data indicate that *K. lactis* Xrn1 is monomeric in solution. Human Xrn1 contains only 70 residues for this segment, which is much shorter than that in *K. lactis* Xrn1 (150 residues; Fig. 1). Therefore, this domain is unlikely to be present in human Xrn1, and may instead be unique to the fungal Xrn1 proteins.

### Comparison to the structure of Rat1/Xrn2

The overall structures of CR1 and CR2 of Xrn1 are similar to the equivalent regions of Rat1/Xrn2 (Fig. 2c), consistent with their high degree of sequence conservation (Supplementary Fig. 1). The r.m.s. distance for 437 equivalent Cα atoms of CR1 and CR2 between the two structures is 1.4 Å. Most of the central β-sheet and its surrounding helices of CR1 have the same conformation in the two structures. However, helices αB and αD, as well as several connecting loops (for example the β5–αG segment), have clear differences between the two structures (Fig. 2c). Another important structural difference concerns the tower domain (helix αD) in Rat1/Xrn2. The equivalent helix in Xrn1 is shorter, and Xrn1 does not have a pronounced structural feature in this region, consistent with earlier suggestions based on sequence analysis<sup>26</sup>.

The 60-residue segment that directly follows CR2 in Xrn1 (residues 674–731) forms a structure that shows general similarity to that of the equivalent segment in Rat1/Xrn2 (Fig. 2c). The N-terminal part of this segment covers up one edge of CR1, and the C-terminal part traverses the bottom of CR1, although its exact location is noticeably different from that of Rat1/Xrn2 (Supplementary Fig. 3).

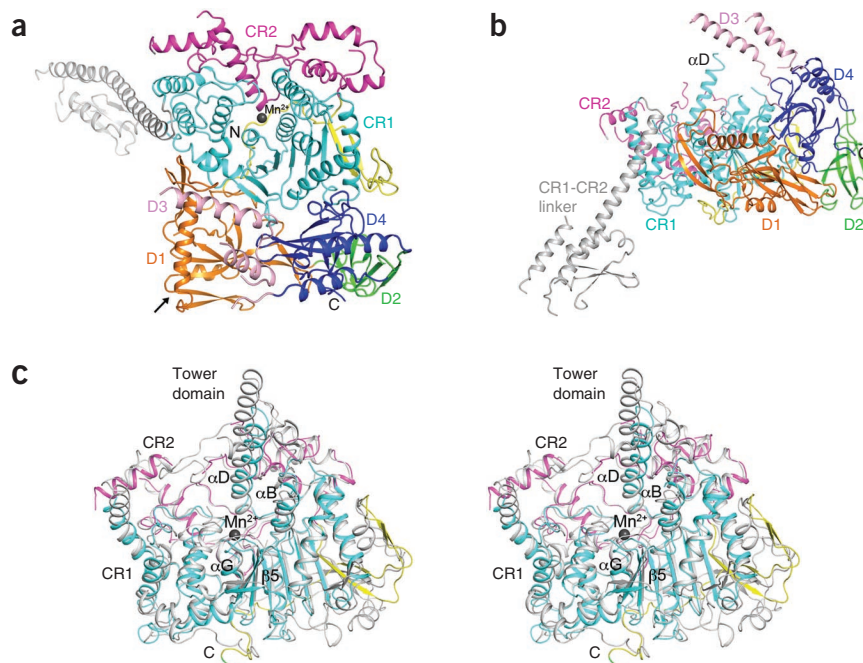
**Table 1** Summary of crystallographic information

Structure	<i>K. lactis</i> Xrn1 E178Q mutant	E178Q mutant in complex with Mn <sup>2+</sup>
<b>Data collection</b>		
Space group	<i>P</i> 1	<i>P</i> 1
Cell dimensions		
<i>a</i> , <i>b</i> , <i>c</i> (Å)	115.7, 132.3, 143.9	116.3, 132.6, 144.1
α, β, γ (°)	110.1, 105.7, 103.7	109.9, 105.8, 104.0
Resolution (Å)*	30–2.9 (3.0–2.9)	30–2.9 (3.0–2.9)
<i>R</i> <sub>merge</sub> (%)	4.5 (25.8)	6.4 (45.8)
<i>I</i> /σ <i>I</i>	15.8 (2.7)	8.8 (1.4)
Completeness (%)	97 (96)	96 (90)
Redundancy	2.0 (2.0)	2.0 (2.0)
<b>Refinement</b>		
Resolution	30–2.9	30–2.9
No. of reflections	146,829	143,344
<i>R</i> <sub>work</sub> / <i>R</i> <sub>free</sub> (%)	24.1 / 30.5	24.8 / 28.4
No. atoms		
Protein	34,041	34,041
Ligand/ion	0	4
<i>B</i> -factors		
Protein	72	80
Ligand/ion	–	69
R.m.s. deviations		
Bond lengths (Å)	0.016	0.017
Bond angles (°)	1.7	1.8

\*The numbers in parentheses are for the highest-resolution shell. One crystal was used for each dataset.

**Figure 2** Structure of *K. lactis* Xrn1.

(a) Schematic drawing of the structure of *K. lactis* Xrn1. The domains are colored as in **Figure 1** and labeled. The Mn<sup>2+</sup> ion in the active site is shown as a dark gray sphere. (b). Structure of *K. lactis* Xrn1, viewed along the arrow indicated in **a**. (c) Stereoview of overlay of *K. lactis* Xrn1 and *S. pombe* Rat1/Xrn2 structures<sup>26</sup>. For simplicity, the linker between CR1 and CR2 and domains D1–D4 of Xrn1 are not shown. The structure of Xrn1 is colored as in **a**, and that of Rat1/Xrn2 is in gray. All the structure figures were produced with PyMOL (<http://www.pymol.org>) unless stated otherwise.



This segment of Rat1/Xrn2 also mediates interactions with Rai1 (ref. 26). The structural and amino acid sequence differences in this region of Xrn1 therefore define the molecular basis of why it cannot interact with Rai1.

### Unique structural features of Xrn1

In addition to the structural differences between Xrn1 and Rat1/Xrn2 described above, Xrn1 contains a 510-residue C-terminal extension that is absent from Rat1/Xrn2 (**Fig. 1**).

Our structure shows that these residues form three distinct domains (D1, D2 and D4), with possibly another domain (D3) that is mostly disordered in the current crystal (**Fig. 2a**). Residues in domains D1 and D4 cover up one side of CR1, but the four domains are located more than 20 Å away from the active site of Xrn1.

Unexpectedly, domains D1, D2 and D4 contain a similar central, five-stranded  $\beta$ -barrel core, with an r.m.s. distance of 1.4 Å for approximately 40 equivalent C $\alpha$  atoms (**Supplementary Fig. 4**). The sequence identity among these structurally equivalent residues is only about 15%. The backbone fold of this  $\beta$ -barrel core is related to that of tudor domains, chromo domains and others<sup>30</sup>, based on a DaliLite search through the PDB<sup>31</sup>. Most of these domains are involved in protein-protein interactions, some of which are mediated through methylated lysines. However, the cluster of aromatic residues in tudor and chromo domains that is important for binding methylated lysines is absent from Xrn1, suggesting that these Xrn1 domains are unlikely to recognize methylated proteins.

The structure of domain D1, formed by residues 732–914, also contains several additional features in the periphery, including two three-stranded  $\beta$ -sheets and two helices (**Fig. 3a**). The closest

structural homolog for its central  $\beta$ -barrel core is the chromo-domain of *S. cerevisiae* Eaf3 (**Supplementary Fig. 4**)<sup>32,33</sup>. However, the Z score from DaliLite is 6.5, and the sequence identity for structurally equivalent residues is 12%, suggesting that the homology is weak.

Domain D2 is formed by two stretches of Xrn1, residues 915–960 and 1,134–1,151 (**Fig. 3b**), as there is an insert (residues 961–1,133) between the third and fourth strands of the  $\beta$ -barrel. This domain has intimate interactions with domain D4 but does not contact CR1 directly. Domain D4 is formed by residues 1,152–1,240 as well as residues 961–978 and 1,110–1,133 at the two ends of the insert in D2 (**Fig. 3b**). The closest structural homologs of these two domains include a tudor domain in JMJD2A<sup>34</sup>, a domain in the transcription anti-termination factor NusG<sup>35,36</sup>, the N-terminal domain of type II restriction endonuclease Hpy99I<sup>37</sup>, and the CPH domain of Cul7 and PARC<sup>38</sup> (**Supplementary Fig. 5**). The Z scores of these structural comparisons are ~6.5, with sequence identities of ~15%.

As domains D2 and D4 have strong interactions with each other, they are reminiscent of the double tudor domains that have been observed in some proteins, such as 53BP1 (refs. 39,40) and Crb2 (ref. 41). However, structural overlays show that the relative orientations and positions of domains D2 and D4 in Xrn1 are different from those in these other double tudor domains.

Domains D1 and D4 have close contacts with CR1 (**Fig. 2a**), burying roughly 2,000 Å<sup>2</sup> of surface area in this interface (**Supplementary Fig. 1**). One of the three-stranded  $\beta$ -sheets in the periphery of domain D1 interacts with the N-terminal segment (helix  $\alpha$ A and strand  $\beta$ 1) and helix  $\alpha$ H of CR1 (**Fig. 3a**). Domain D4 primarily interacts with the loop after  $\beta$ 1, helix  $\alpha$ C and the  $\beta$ 6– $\beta$ 7 loop in CR1 (**Fig. 3b**).

The current structure leads us to suggest that there is another domain (D3). This domain is formed by residues 979–1,109 in the insert of domain D2 (**Fig. 1**). Two helical segments of this domain can be modeled in three of the four Xrn1 molecules. These two helices are positioned far away from the rest of the structure (**Fig. 2b**) and show large structural differences among the Xrn1 molecules. Residues in this putative domain show reasonable conservation between human and yeast Xrn1 (**Supplementary Fig. 1**), suggesting that it may also have a role in Xrn1 function (see below).

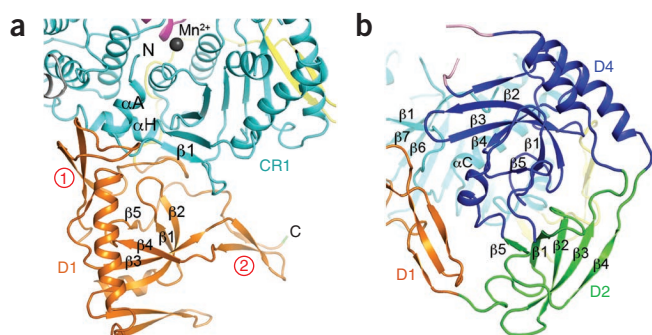
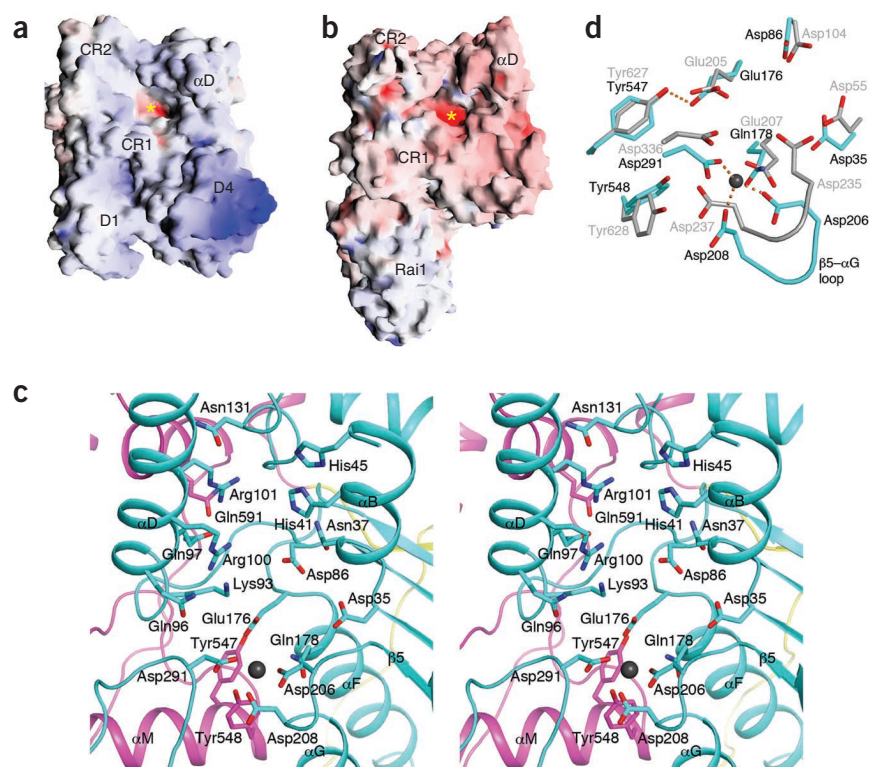


**Figure 3** Unique structural features in Xrn1. (a) Close-up of the structure of domain D1, as well as its interactions with CR1. The two three-stranded  $\beta$ -sheets in the periphery of the structure are labeled with the circled numbers in red. (b) Close-up of the structure of domains D2 and D4, as well as the interactions between D4 and CR1.

**Figure 4** Structure of the active site of *K. lactis* Xrn1. **(a)** Molecular surface of *K. lactis* Xrn1, colored by electrostatic potential. The active site region is indicated with the yellow star. Domain D3 and the linker between CR1 and CR2 are not shown. **(b)** Molecular surface of *S. pombe* Rat1–Rai1 complex<sup>26</sup>, viewed in the same orientation as **a**. Panels **a** and **b** were produced with the program Grasp<sup>50</sup>. **(c)** Stereo drawing of the active site of *K. lactis* Xrn1. Side chains in the active site are shown as stick models and labeled. The bound Mn<sup>2+</sup> ion is shown as a gray sphere. **(d)** Overlay of the structures of the seven conserved acidic residues in CR1 and the two Tyr residues in CR2 in the active sites of Xrn1 (in cyan for carbon atoms) and Rat1/Xrn2 (in gray). The liganding interactions of the Mn<sup>2+</sup> ion are indicated with dashed lines. Residues in Xrn1 are labeled in black, and those in Rat1/Xrn2 labeled in gray.



### The active site of Xrn1

The active site of Xrn1 is located in a deep pocket near the bottom of the  $\alpha$ D helix in CR1 (Fig. 4a). As in Rat1/Xrn2 (ref. 26), CR2 encircles the active site in Xrn1 but makes few direct contributions to it (Fig. 4b). Nonetheless, this active site landscape probably explains why the XRNs are exoribonucleases. The location of the active site in a pocket is unlikely to be compatible with an endonuclease activity. Domains D1–D4 are located far from the active site. The amino acid sequences of these four domains contain an excess of basic residues (the pI of the entire 510-residue segment is about 10), as also indicated by the positively charged surface patches in domain D4 (Fig. 4a), which suggests that these domains might help to bind the RNA substrate. In comparison, the molecular surface of Rat1/Xrn2 is more electronegative in nature (Fig. 4b). The pI for the conserved regions of Xrn1 and Rat1/Xrn2 is about 5.5 (ref. 23).

Almost all the residues in the active site region are highly conserved among the XRNs (Supplementary Fig. 1). The seven conserved acidic residues correspond to Asp35, Asp86, Glu176, Glu178, Asp206, Asp208 and Asp291 in *K. lactis* Xrn1 (Fig. 4c). The N-terminal end of helix  $\alpha$ D provides several positive (lysine and arginine) and hydrophilic (glutamine) residues to the active site. Helix  $\alpha$ B also contributes several hydrophilic residues to the active site. Only three side chains in CR2—Tyr547, Tyr548 and Gln591—are located near the active site (Fig. 4c), and all three residues are conserved among the XRNs.

By co-crystallizing the E178Q mutant with 5 mM MnCl<sub>2</sub> (Table 1), we could observe the binding of one Mn<sup>2+</sup> ion in the active site (Fig. 4c). The metal ion is tightly coordinated by the side chains of three of the conserved acidic residues—Asp206, Asp208 and Asp291 (Fig. 4d)—with distances of roughly 2.1 Å. There are no conformational changes in the enzyme upon the binding of this cation.

### Domain D1 is required for nuclease activity

We next assessed the functional importance of the Xrn1-specific domains observed in the structure. We created three internal deletion mutants, removing residues 355–492 (the linker between CR1 and CR2), 993–1,098 (domain D3) and 927–1,145 (domains D2 and D3), as well as two C-terminal truncations, removing residues 752–1,453 (from domain D1 onward) and 916–1,453

(from domain D2 onward) of *K. lactis* Xrn1. The structure suggests that removing D3 or D2 and D3 is unlikely to have a large impact on the interactions of domains D1 and D4 with the rest of the structure (especially CR1; Fig. 2a). All these mutants were expressed in and purified from *Escherichia coli*. All gave clean gel-filtration profiles (Supplementary Fig. 6), suggesting that the deletions did not affect the overall folding of the protein. Exonuclease activity was measured using a 240-nt RNA substrate labeled at its 3'-end as well as a 55-nt single-stranded DNA substrate labeled at its 5'-end. Wild-type *K. lactis* Xrn1 (residues 1–1,245) showed strong, time-dependent degradation of the RNA substrate (Fig. 5a). The activity seemed to be mostly processive, as there was little evidence for intermediates in the reaction.

We next analyzed the nuclease activity of the mutants. Deleting domain D3 or D2 and D3 essentially abolished nuclease activity toward the RNA substrate (Fig. 5b). On the other hand, the domain in the linker segment between CR1 and CR2 was not required for activity (Fig. 5b), consistent with its poor conservation among the XRNs. We also introduced a double mutation, K388A K389A, in the long helix in this region, and it had little impact on nuclease activity. The truncation mutant that lacked all four domains ( $\Delta$ 752–C terminus) was inactive (Fig. 5b). By contrast, the truncation mutant that lacked domains D2–D4 ( $\Delta$ 916–C terminus) showed weak nuclease activity. To assess the nuclease activity of the proteins more carefully, we followed the reactions in a time course. The data confirmed that the mutant lacking the linker segment between CR1 and CR2 had slightly lower activity than the wild-type enzyme, whereas the derivative lacking domains D2–D4 had much lower activity (Supplementary Fig. 7).

We further characterized the nuclease activity of wild-type Xrn1 and the deletion mutants using the ssDNA substrate. Earlier studies showed that yeast Xrn1 has nuclease activity toward ssDNA<sup>23,24,28</sup>. Wild-type *K. lactis* Xrn1 readily degraded the ssDNA substrate, whereas the truncation mutant that lacked all four domains ( $\Delta$ 752–C

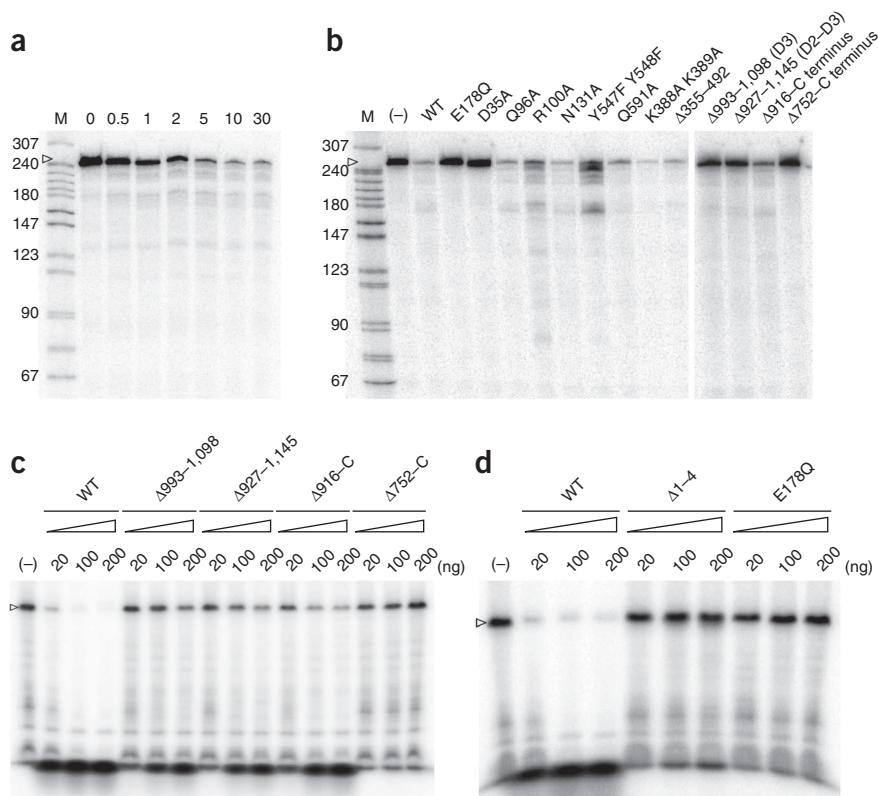


**Figure 5** Biochemical studies on the nuclease activity of *K. lactis* Xrn1. **(a)** Time course showing the degradation of the 240-nt RNA substrate (indicated with the arrowhead, with 5'-end monophosphate and labeled at the 3'-end) by recombinant *K. lactis* Xrn1 (residues 1–1,245). **(b)** RNase assays showing the effect of site-specific and deletion mutations on the activity of *K. lactis* Xrn1. All reactions contained 20 ng of enzyme, except for the four lanes at the right, which contained 50 ng of enzyme. **(c)** Nuclease assays showing the effect of C-terminal deletion mutations on the activity of *K. lactis* Xrn1 toward a 55-nt ssDNA substrate, labeled at the 5'-end. **(d)** Nuclease assays showing the effect of deleting the N-terminal four residues on the activity of *K. lactis* Xrn1 toward the 55-nt ssDNA substrate.

activity. Domains D2–D4 might help to maintain domain D1 in the correct conformation, thereby indirectly stabilizing the conformation of the N-terminal segment.

We carried out additional experiments to characterize other possible molecular mechanism(s) for the reduced activity of the deletion mutants, including electrophoretic mobility shift assays and thermal shift experiments<sup>42</sup>. The mutations weakened but did not disrupt binding of the 240-nt RNA (Fig. 6).

terminus) was essentially inactive (Fig. 5c). On the other hand, the truncation mutant that lacked domains D2–D4 (Δ916–C terminus) and the two internal deletion mutants showed weak activity.

We also assessed the functional importance of the highly conserved residues in the active site of Xrn1 (and Xrn2). Many of them, especially those in CR1, have been examined earlier by mutagenesis studies<sup>23,24</sup>. We selected several additional conserved residues in the active site for study, especially the three conserved residues in CR2 that make contributions to the active site—Tyr547, Tyr548 and Gln591 (Fig. 4c). The experiments confirmed that the E178Q mutant had essentially no nuclease activity (Fig. 5b). The D35A mutation also abolished activity. The R100A and Y547A Y548A mutants maintained some activity toward the RNA substrate, although they both showed the presence of intermediates in comparison to the wild-type enzyme. Finally, the Q96A, N131A and Q591A mutations had only small effects on nuclease activity, as confirmed by time course experiments (Supplementary Fig. 7).

### Domain D1 may stabilize the N-terminal segment

The crystal structure suggests a possible explanation for the functional importance of domain D1. It has close interactions with the N-terminal segment, and the N terminus is located near the active site (Fig. 3a). Therefore, domain D1 may help to define or stabilize the conformation of the N-terminal segment, which might be important for Xrn1 catalysis.

To assess the functional importance of the N-terminal segment of Xrn1 for its nuclease activity, we created a deletion mutant that removed the first four residues (Δ1–4) (Fig. 3a and Supplementary Fig. 1). The mutant was purified following the same protocol as above and behaved the same on a gel-filtration column as wild-type Xrn1. However, this mutant had markedly reduced nuclease activity toward the 55-nt ssDNA substrate (Fig. 5d). The experimental data are consistent with our model for why domain D1 is required for nuclease

The RNA substrate seemed to be able to bind multiple copies of Xrn1, resulting in a complex that failed to migrate into the gel for the wild-type enzyme at higher concentrations (Fig. 6). By contrast, several intermediate complexes were observed with the mutants, probably because the mutants had weaker affinity for the RNA. These data suggest that the four Xrn1-specific domains contribute to RNA binding, which may be important for recruiting substrate and possibly for other functions.

The mutations also reduced the thermal stability of the enzyme (Supplementary Fig. 8). Therefore, the Xrn1-specific domains might

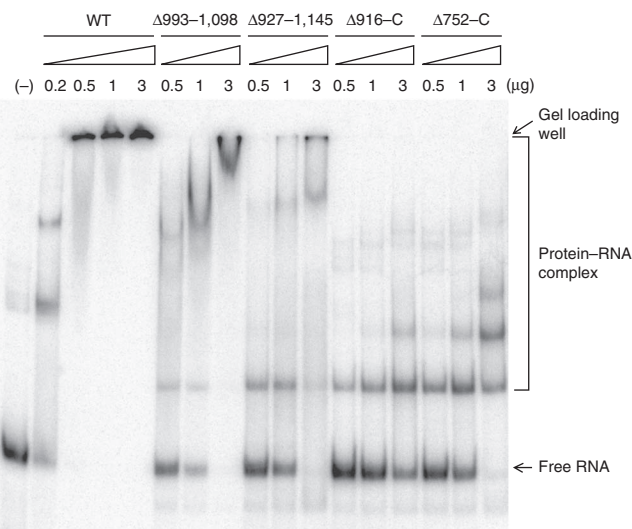


**Figure 6** RNA binding activity of *K. lactis* Xrn1. Electrophoretic mobility shift assays for wild-type and various deletion mutants of Xrn1. The wild-type enzyme has high affinity for the 240-nt RNA, producing a large complex that did not migrate into the gel.

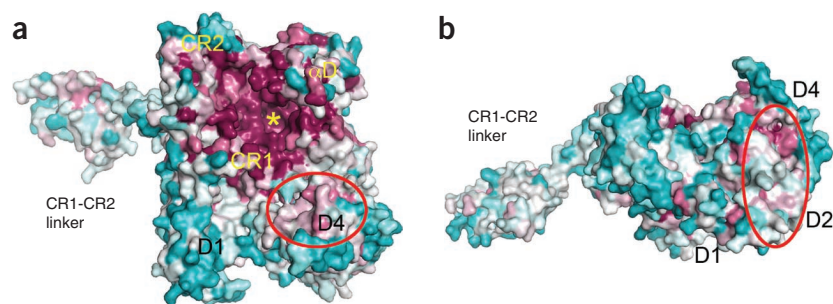


**Figure 7** Conserved surface features in the structure of *K. lactis* Xrn1. (a) Molecular surface of *K. lactis* Xrn1 colored by sequence conservation among fungal and mammalian enzymes, analyzed by the program ConSurf<sup>51</sup>. The colors vary from dark purple for highly conserved residues to cyan for residues with little conservation. A weakly conserved surface patch is highlighted with the red oval. (b) Surface conservation of Xrn1, viewed after a 90° rotation around the horizontal axis from a.

also stabilize the overall structure of Xrn1, facilitating its catalysis. This is somewhat reminiscent of Rat1/Xrn2, as Rai1 can stimulate Rat1 nuclease activity by binding and stabilizing its overall structure<sup>26,27</sup>. At the same time, the mutant that lacked the CR1–CR2 linker also had reduced thermal stability but was nonetheless fully active (Fig. 5b), suggesting that there is not a direct correlation between stability and nuclease activity.

## DISCUSSION

We report the crystal structure of an Xrn1 enzyme, which shows that the 510-residue segment that is unique to Xrn1 forms four distinct domains. Biochemical data show that these domains are important for catalysis by Xrn1, even though they are located far from the active site and are only weakly conserved among the Xrn1 enzymes. Therefore, the highly conserved core of the XRNs (CR1 and CR2) is not sufficient for enzyme activity, and requires the help of less conserved segments (or another protein, such as Rai1 in the case of Rat1/Xrn2) for stability or activity.

The four Xrn1-specific domains probably have other important functions besides catalysis. Xrn1 interacts with many proteins during its functions in RNA metabolism<sup>5</sup>, and the new domains might constitute a platform for the recruitment of these other proteins. Two weakly conserved surface patches can be identified in domains D1, D2 and D4 (Fig. 7a,b). The conserved surface patches may mediate interactions with these other proteins or with the substrate of Xrn1.

The position and coordination pattern of the Mn<sup>2+</sup> ion in Xrn1 seem to be unique among enzymes with homologous structures (Supplementary Fig. 9). The observed positions of the metal ions are highly variable in these other enzymes<sup>43</sup>, including bacteriophage T4 RNase H<sup>44</sup> and flap endonucleases<sup>45–48</sup>. The distances between the metal ions and their ligands in these other structures are often 3 Å (or more), too far for liganding interactions. Our inability to observe binding of a predicted second metal ion to the E178Q mutant suggests that the mutation may have disrupted the other binding site (Supplementary Fig. 9).

Although most of the residues in the active sites of Xrn1 and Rat1/Xrn2 are conserved (Supplementary Fig. 1), the positions and conformations of many of these residues show clear differences between the two structures. For example, the two conserved acidic residues that coordinate the Mn<sup>2+</sup> ion in our structure—Asp206 and Asp208—have conformational differences in both their main-chain (β5–αG loop) and side-chain atoms when compared with Rat1/Xrn2 (Fig. 4d). As a consequence, the Mn<sup>2+</sup> ion observed in the Xrn1

structure cannot maintain a similar binding mode in Rat1/Xrn2 unless there is a conformational change in the latter.

A collection of missense mutations in Xrn1 that had severely reduced nuclease activity has been identified from a genetic screen<sup>23</sup>. Most of these mutations are in CR1 and are located in the active site of Xrn1 (Fig. 4c). Three additional mutations—C201R, L592P and W798R—are located in the hydrophobic core of the structure. Therefore, all of these mutations either directly disrupt the active site or indirectly disturb the overall structure of the enzyme.

Our biochemical data indicate that domain D1 is required for the nuclease activity of Xrn1, whereas domains D2–D4 are important but

might not be essential for catalysis. Earlier deletion studies with yeast Xrn1 were based on a truncation that started in the middle of domain D4 (ref. 23), which probably caused the unfolding of this domain and may in turn have had detrimental effects on the other domains.

The four Xrn1-specific domains cover up one side of CR1 (Fig. 2a), whereas Rai1 is located at the bottom of CR1 in the complex with Rat1/Xrn2 (ref. 26) (Fig. 4b). Therefore, the relative positions of the four domains in Xrn1 are entirely different from those of Rai1. In addition, our biochemical and functional studies showed that Rai1 has RNA 5′-end pyrophosphohydrolase and decapping activities, which are important for RNA 5′-end capping quality control<sup>26,49</sup>. In comparison, the four domains in Xrn1 are unlikely to have any catalytic activity. On the other hand, Rai1 can indirectly enhance the activity of Rat1/Xrn2, possibly by stabilizing the overall structure of the enzyme<sup>26,27</sup>. In that regard, it would be interesting to investigate whether the protein partners of Xrn1, possibly recruited through the four Xrn1-specific domains, can also regulate the exoribonuclease activity of this enzyme.

## METHODS

Methods and any associated references are available in the online version of the paper at <http://www.nature.com/nsmb/>.

**Accession codes.** The atomic coordinates have been deposited at the Protein Data Bank, with accession codes 3PIE and 3PIF.

*Note: Supplementary information is available on the Nature Structural & Molecular Biology website.*

## ACKNOWLEDGMENTS

We thank N. Whalen and S. Myers for setting up the X29A beamline at the National Synchrotron Light Source (NSLS). This research was supported in part by grants from the US National Institutes of Health to L.T. (GM090059 and GM077175) and J.L.M. (GM028983).

## AUTHOR CONTRIBUTIONS

J.H.C. and S.X. carried out protein expression, purification and crystallization experiments. J.H.C., S.X. and L.T. carried out crystallographic data collection, structure determination and refinement. J.H.C. carried out mutagenesis, nuclease assays, EMSA and thermal shift experiments. K.X. helped with the preparation of the nuclease substrate. J.L.M. designed experiments and analyzed data. All authors commented on the manuscript. L.T. designed experiments, analyzed data and wrote the paper.

## COMPETING FINANCIAL INTERESTS

The authors declare no competing financial interests.

Published online at <http://www.nature.com/nsmb/>.

Reprints and permissions information is available online at <http://npg.nature.com/reprintsandpermissions/>.

- Parker, R. & Song, H. The enzymes and control of eukaryotic mRNA turnover. *Nat. Struct. Mol. Biol.* **11**, 121–127 (2004).
- Newbury, S.F. Control of mRNA stability in eukaryotes. *Biochem. Soc. Trans.* **34**, 30–34 (2006).
- Bousquet-Antonelli, C., Presutti, C. & Tollervey, D. Identification of a regulated pathway for nuclear pre-mRNA turnover. *Cell* **102**, 765–775 (2000).
- Gatfield, D. & Izaurralde, E. Nonsense-mediated messenger RNA decay is initiated by endonucleolytic cleavage in *Drosophila*. *Nature* **429**, 575–578 (2004).
- Coller, J. & Parker, R. Eukaryotic mRNA decapping. *Annu. Rev. Biochem.* **73**, 861–890 (2004).
- Zabolotskaya, M.V., Grima, D.P., Lin, M.-D., Chou, T.-B. & Newbury, S.F. The 5'→3' exoribonuclease Pacman is required for normal male fertility and is dynamically localized in cytoplasmic particles in *Drosophila* testis cells. *Biochem. J.* **416**, 327–335 (2008).
- Amberg, D.C., Goldstein, A.L. & Cole, C.N. Isolation and characterization of RAT1: an essential gene of *Saccharomyces cerevisiae* required for the efficient nucleocytoplasmic trafficking of mRNA. *Genes Dev.* **6**, 1173–1189 (1992).
- Kenna, M., Stevens, A., McCammon, M. & Douglas, M.G. An essential yeast gene with homology to the exonuclease-encoding XRN1/KEM1 gene also encodes a protein with exoribonuclease activity. *Mol. Cell. Biol.* **13**, 341–350 (1993).
- di Segni, G., McConaughy, B.L., Shapiro, R.A., Aldrich, T.L. & Hall, B.D. TAP1, a yeast gene that activates the expression of a tRNA gene with a defective internal promoter. *Mol. Cell. Biol.* **13**, 3424–3433 (1993).
- Kim, M. *et al.* The yeast Rat1 exonuclease promotes transcription termination by RNA polymerase II. *Nature* **432**, 517–522 (2004).
- West, S., Gromak, N. & Proudfoot, N.J. Human 5'→3' exonuclease Xrn2 promotes transcription termination at co-transcriptional cleavage sites. *Nature* **432**, 522–525 (2004).
- Luo, W., Johnson, A.W. & Bentley, D.L. The role of Rat1 in coupling mRNA 3'-end processing to transcription termination: implications for a unified allosteric-torpedo model. *Genes Dev.* **20**, 954–965 (2006).
- Kaneko, S., Rozenblatt-Rosen, O., Meyerson, M. & Manley, J.L. The multifunctional protein p54<sup>nrB</sup>/PSF recruits the exonuclease XRN2 to facilitate pre-mRNA 3' processing and transcription termination. *Genes Dev.* **21**, 1779–1789 (2007).
- El Hage, A., Koper, M., Kufel, J. & Tollervey, D. Efficient termination of transcription by RNA polymerase I requires the 5' exonuclease Rat1 in yeast. *Genes Dev.* **22**, 1069–1081 (2008).
- Kawauchi, J., Mischo, H., Braglia, P., Rondon, A. & Proudfoot, N.J. Budding yeast RNA polymerases I and II employ parallel mechanisms of transcriptional termination. *Genes Dev.* **22**, 1082–1092 (2008).
- Luke, B. *et al.* The Rat1p 5' to 3' exonuclease degrades telomeric repeat-containing RNA and promotes telomere elongation in *Saccharomyces cerevisiae*. *Mol. Cell* **32**, 465–477 (2008).
- Chernyakov, I., Whipple, J.M., Kotelawala, L., Grayhack, E.J. & Phizicky, E.M. Degradation of several hypomodified mature tRNA species in *Saccharomyces cerevisiae* is mediated by Met22 and the 5'→3' exonucleases Rat1 and Xrn1. *Genes Dev.* **22**, 1369–1380 (2008).
- Shobuike, T., Tatebayashi, K., Tani, T., Sugano, S. & Ikeda, H. The dhp1+ gene, encoding a putative nuclear 5'→3' exoribonuclease, is required for proper chromosome segregation in fission yeast. *Nucleic Acids Res.* **29**, 1326–1333 (2001).
- Gy, I. *et al.* *Arabidopsis* FIERY1, XRN2, and XRN3 are endogenous RNA silencing suppressors. *Plant Cell* **19**, 3451–3461 (2007).
- Olmedo, G. *et al.* Ethylene-insensitive5 encodes a 5'→3' exoribonuclease required for regulation of the EIN3-targeting F-box proteins EBF1/2. *Proc. Natl. Acad. Sci. USA* **103**, 13286–13293 (2006).
- Potuschak, T. *et al.* The exoribonuclease XRN4 is a component of the ethylene response pathway in *Arabidopsis*. *Plant Cell* **18**, 3047–3057 (2006).
- Gazzani, S., Lawrenson, T., Woodward, C., Headon, D. & Sablowski, R. A link between mRNA turnover and RNA interference in *Arabidopsis*. *Science* **306**, 1046–1048 (2004).
- Page, A.M., Davis, K., Molineux, C., Kolodner, R.D. & Johnson, A.W. Mutational analysis of exoribonuclease I from *Saccharomyces cerevisiae*. *Nucleic Acids Res.* **26**, 3707–3716 (1998).
- Solinger, J.A., Pascolini, D. & Heyer, W.-D. Active-site mutations in the Xrn1p exoribonuclease of *Saccharomyces cerevisiae* reveal a specific role in meiosis. *Mol. Cell. Biol.* **19**, 5930–5942 (1999).
- Yang, W., Lee, J.Y. & Nowotny, M. Making and breaking nucleic acids: Two-Mg<sup>2+</sup>-ion catalysis and substrate specificity. *Mol. Cell* **22**, 5–13 (2006).
- Xiang, S. *et al.* Structure and function of the 5'→3' exoribonuclease Rat1 and its activating partner Rai1. *Nature* **458**, 784–788 (2009).
- Xue, Y. *et al.* *Saccharomyces cerevisiae* Rai1 (YGL246c) is homologous to human DOM3Z and encodes a protein that binds the nuclear exoribonuclease Rat1p. *Mol. Cell. Biol.* **20**, 4006–4015 (2000).
- Stevens, A. & Poole, T.L. 5'-exonuclease-2 of *Saccharomyces cerevisiae*. Purification and features of ribonuclease activity with comparison to 5'-exonuclease-1. *J. Biol. Chem.* **270**, 16063–16069 (1995).
- Hendrickson, W.A. Determination of macromolecular structures from anomalous diffraction of synchrotron radiation. *Science* **254**, 51–58 (1991).
- Maurer-Stroh, S. *et al.* The tudor domain 'royal family': tudor, plant Agenet, chromo, PWWP and MBT domains. *Trends Biochem. Sci.* **28**, 69–74 (2003).
- Holm, L., Kaariainen, S., Rosenstrom, P. & Schenkel, A. Searching protein structure databases with DALI Lite v.3. *Bioinformatics* **24**, 2780–2781 (2008).
- Sun, B. *et al.* Molecular basis of the interaction of *Saccharomyces cerevisiae* Eaf3 chromo domain with methylated H3K36. *J. Biol. Chem.* **283**, 36504–36512 (2008).
- Xu, C., Cui, G., Botuyan, M.V. & Mer, G. Structural basis for the recognition of methylated histone H3K36 by the Eaf3 subunit of histone deacetylase complex Rpd3S. *Structure* **16**, 1740–1750 (2008).
- Huang, Y., Fang, J., Bedford, M.T., Zhang, Y. & Xu, R.-M. Recognition of histone H3 lysine-4 methylation by the double tudor domain of JMJD2A. *Science* **312**, 748–751 (2006).
- Steiner, T., Kaiser, J.T., Marinkovic, S., Huber, R. & Wahl, M.C. Crystal structures of transcription factor NusG in light of its nucleic acid- and protein-binding activities. *EMBO J.* **21**, 4641–4653 (2002).
- Burmann, B.M. *et al.* A NusE:NusG complex links transcription and translation. *Science* **328**, 501–504 (2010).
- Sokolowska, M., Czapińska, H. & Bochtler, M. Crystal structure of the bba-Me type II restriction endonuclease Hpy99I with target DNA. *Nucleic Acids Res.* **37**, 3799–3810 (2009).
- Kaustov, L. *et al.* The conserved CPH domains of Cul7 and PARC are protein-protein interaction modules that bind the tetramerization domain of p53. *J. Biol. Chem.* **282**, 11300–11307 (2007).
- Huyen, Y. *et al.* Methylated lysine 79 of histone H3 targets 53BP1 to DNA double-strand breaks. *Nature* **432**, 406–411 (2004).
- Charier, G. *et al.* The tudor tandem of 53BP1: A new structural motif involved in DNA and RG-rich peptide binding. *Structure* **12**, 1551–1562 (2004).
- Botuyan, M.V. *et al.* Structural basis for the methylation state-specific recognition of histone H4-K20 by 53BP1 and Crb2 in DNA repair. *Cell* **127**, 1361–1373 (2006).
- Vedadi, M. *et al.* Chemical screening methods to identify ligands that promote protein stability, protein crystallization, and structure determination. *Proc. Natl. Acad. Sci. USA* **103**, 15835–15840 (2006).
- Syson, K. *et al.* Three metal ions participate in the reaction catalyzed by T5 Flap endonuclease. *J. Biol. Chem.* **283**, 28741–28746 (2008).
- Mueser, T.C., Nossal, N.G. & Hyde, C.C. Structure of bacteriophage T4 RNase H, a 5' to 3' RNA-DNA and DNA-DNA exonuclease with sequence similarity to the RAD2 family of eukaryotic proteins. *Cell* **85**, 1101–1112 (1996).
- Hwang, K.Y., Baek, K., Kim, H.-Y. & Cho, Y. The crystal structure of flap endonuclease-1 from *Methanococcus jannaschii*. *Nat. Struct. Biol.* **5**, 707–713 (1998).
- Feng, M. *et al.* Roles of divalent metal ions in flap endonuclease-substrate interactions. *Nat. Struct. Mol. Biol.* **11**, 450–456 (2004).
- Sakurai, S. *et al.* Structural basis for recruitment of human flap endonuclease 1 to PCNA. *EMBO J.* **24**, 683–693 (2005).
- Doré, A.S. *et al.* Structure of an archaeal PCNA1-PCNA2-FEN1 complex: elucidating PCNA subunit and client enzyme specificity. *Nucleic Acids Res.* **34**, 4515–4526 (2006).
- Jiao, X. *et al.* Identification of a quality-control mechanism for mRNA 5'-end capping. *Nature* **467**, 608–611 (2010).
- Nicholls, A., Sharp, K.A. & Honig, B. Protein folding and association: insights from the interfacial and thermodynamic properties of hydrocarbons. *Proteins* **11**, 281–296 (1991).
- Armon, A., Graur, D. & Ben-Tal, N. ConSurf: an algorithmic tool for the identification of functional regions in proteins by surface mapping of phylogenetic information. *J. Mol. Biol.* **307**, 447–463 (2001).

## ONLINE METHODS

**Protein expression and purification.** Residues 1–1,245 of *K. lactis* Xrn1 were subcloned into the pET26b vector (Novagen). The expression construct contained a C-terminal hexahistidine tag, which was not removed for crystallization. The native protein was overexpressed overnight in *E. coli* BL21 Star (DE3) cells (Novagen) at 20 °C in the presence of 0.4 mM isopropyl- $\beta$ -D-thiogalactopyranoside (IPTG; Gold Biotechnology, Inc). The soluble protein was eluted from nickel affinity beads (Qiagen) by a buffer containing 20 mM Tris (pH 7.5), 100 mM NaCl, 200 mM imidazole and 10 mM  $\beta$ -mercaptoethanol. The eluted protein was further purified by gel-filtration chromatography and then concentrated to 10 mg ml<sup>-1</sup> in a buffer containing 20 mM Tris (pH 7.5), 200 mM NaCl, 2 mM DTT and 5% (v/v) glycerol. Purified protein samples were flash frozen with liquid nitrogen and then stored at –80 °C.

The selenomethionyl (SeMet) protein was produced in *E. coli* BL21 Star (DE3) cells grown in defined M9 medium supplemented with selenomethionine and specific amino acids to block endogenous methionine biosynthesis<sup>52</sup>. The SeMet protein was purified with the same protocol as the native protein, and the concentration of DTT was increased to 10 mM.

**Protein crystallization.** Crystals were obtained by sitting-drop vapor diffusion at 4 °C. The reservoir solution contained 100 mM Tris (pH 8.5), 0.9 M LiCl and 13.5% (w/v) PEG 6000. The protein solution was supplemented with 0.9 mM Triton X-100, 0.15 mM 1-s-nonyl- $\beta$ -D-thioglucoside and 60 mM Gly-Gly-Gly (Hampton Research) before crystallization. For the Mn<sup>2+</sup> complex, 5 mM MnCl<sub>2</sub> was included in the protein solution. The crystals were flash frozen in liquid nitrogen for diffraction analysis and data collection at 100 K.

**Data collection and processing.** Native and selenomethionyl single-wavelength anomalous diffraction datasets were collected on an ADSC Q315 CCD at the X29A beamline of the National Synchrotron Light Source (NSLS) at Brookhaven National Laboratory. The diffraction images were processed using the HKL package<sup>53</sup>. The crystals belong to space group *P1*, and there are four molecules of Xrn1 in the crystallographic asymmetric unit. The data processing statistics are summarized in **Table 1**.

**Structure determination and refinement.** The initial structure of Xrn1 was determined by the molecular replacement method with the program Phaser<sup>54</sup>, using the structure of *S. pombe* Rat1 as the model (corresponding to the N-terminal 50% of XRN1)<sup>26</sup>. The four molecules of XRN1 were located in the unit cell, although the subsequent electron density map was not of sufficient quality, especially for the C-terminal segment, which was not present in the Rat1 structure. Phase information from the atomic model was combined with the selenomethionyl SAD dataset to produce better phases with the program Phaser, which were further improved by fourfold NCS averaging with the program DM in the CCP4 package<sup>55</sup>. The atomic model was built with the programs O<sup>56</sup> and Coot<sup>57</sup>. The structure refinement was carried out with the programs CNS<sup>58</sup> and Refmac<sup>59</sup>. The statistics on the structure refinement are summarized in **Table 1**.

**ExoRNase assay.** Site-specific mutations were created with the QuikChange kit (Stratagene), and deletion mutations were created by PCR. The mutants were sequenced to confirm correct incorporation of the mutations and purified following the same protocol as the wild-type protein.

To prepare the RNA substrate for exoRNase assays, the plasmid pG3SVL-A, containing the SV40 late (SVL) polyadenylation site, was linearized with DraI

and transcribed with Sp6 RNA polymerase (Promega) for 2 h at 37 °C. The 240-nt RNA transcripts were gel-purified using standard procedures<sup>60</sup>. The 5' termini were dephosphorylated with calf intestinal phosphatase (New England Biolabs) for 2 h at 37 °C and the RNAs were subsequently labeled at their 3'-ends with <sup>32</sup>P Cp and T4 RNA ligase (Promega) overnight at 4 °C. The 5' termini were monophosphorylated by T4 polynucleotide kinase (New England Biolabs) and 1 mM ATP at 37 °C for 2 h.

To prepare the DNA substrate, a 55-nt ssDNA (5'-CTTAAACAGCAAGA AGATCGTTCGTAACGAAAATACTGATACAGTCCGCCTGTATG-3') was purchased from Operon. The 5'-end was labeled with [ $\gamma$ -<sup>32</sup>P]ATP and T4 polynucleotide kinase for 2 h at 37 °C.

ExoRNase assays were performed at 37 °C for 30 min or as indicated. Reaction mixtures (20- $\mu$ l volume) contained either 3'-end labeled RNA (~100 counts per second) or 5'-end labeled ssDNA (100 ng) as a substrate, 50 mM NaCl, 10 mM MgCl<sub>2</sub>, 20 mM Tris (pH 8.0), 0.5 mM DTT, 50  $\mu$ g ml<sup>-1</sup> BSA, 1 U RNasin and 20 or 50 ng of recombinant Xrn1. RNA products were isolated by phenol/chloroform extraction and ethanol precipitation and fractionated by PAGE using a gel with 10% acrylamide and 7 M urea. The data were analyzed by PhosphorImager. Assays were repeated several times to ensure reproducibility.

**Electrophoretic mobility shift assay.** Reaction mixtures (10  $\mu$ l) containing the 3'-end labeled 240-nt RNA (~100 counts per second) in binding buffer (25 mM Tris (pH 7.5), 200 mM NaCl, 2 mM DTT, 0.5 mM EDTA) and indicating amount of protein were incubated at room temperature for 30 min and then fractionated using a 6% native polyacrylamide gel at 4 °C. The data were visualized by PhosphorImager.

**Thermal shift assay.** Thermal stabilities of wild-type and truncated mutant Xrn1 proteins were analyzed at various temperatures by the Mx3005P Real-Time PCR system (Stratagene). Each protein (4–10  $\mu$ M) was mixed with fluorescence dye (SYPRO orange; Invitrogen), for monitoring conformational changes in 20 mM Tris (pH 7.5), 200 mM NaCl and 2 mM DTT. The temperature was increased from 25 to 75 °C over a 50-min period.

- Doublé, S. *et al.* Crystallization and preliminary X-ray analysis of the 9 kDa protein of the mouse signal recognition particle and the selenomethionyl-SRP. *FEBS Lett.* **384**, 219–221 (1996).
- Otwinowski, Z. & Minor, W. Processing of X-ray diffraction data collected in oscillation mode. *Methods Enzymol.* **276**, 307–326 (1997).
- McCoy, A.J. *et al.* Phaser crystallographic software. *J. Appl. Crystallogr.* **40**, 658–674 (2007).
- CCP4. The CCP4 suite: programs for protein crystallography. *Acta Crystallogr. D Biol. Crystallogr.* **50**, 760–763 (1994).
- Jones, T.A., Zou, J.Y., Cowan, S.W. & Kjeldgaard, M. Improved methods for building protein models in electron density maps and the location of errors in these models. *Acta Crystallogr. A* **47**, 110–119 (1991).
- Emsley, P. & Cowtan, K.D. Coot: model-building tools for molecular graphics. *Acta Crystallogr. D Biol. Crystallogr.* **60**, 2126–2132 (2004).
- Brünger, A.T. *et al.* Crystallography & NMR System: A new software suite for macromolecular structure determination. *Acta Crystallogr. D Biol. Crystallogr.* **54**, 905–921 (1998).
- Murshudov, G.N., Vagin, A.A. & Dodson, E.J. Refinement of macromolecular structures by the maximum-likelihood method. *Acta Crystallogr. D Biol. Crystallogr.* **53**, 240–255 (1997).
- Takagaki, Y., Ryner, L.C. & Manley, J.L. Separation and characterization of a Poly(A) polymerase and a cleavage/specificity factor required for pre-mRNA polyadenylation. *Cell* **52**, 731–742 (1988).